

Magnetoelectric coupling through the spin flop transition in Ni_3TeO_6

M. O. Yokosuk,¹ Amal al-Wahish,¹ Sergey Artyukhin,^{2,3} K. R. O'Neal,¹ D. Mazumdar,¹ P. Chen,¹ Junjie Yang,⁴ Yoon Seok Oh,^{2,5} Stephen A. McGill,⁶ K. Haule,² Sang-Wook Cheong,^{2,4,5} David Vanderbilt,² and J. L. Musfeldt^{1,7}

¹*Department of Chemistry, University of Tennessee, Knoxville, Tennessee 37996 USA*

²*Department of Physics and Astronomy, Rutgers University, Piscataway, New Jersey 08854, USA*

³*Quantum Materials Theory, Italian Institute of Technology, Via Morego 30, 16163 Genova, Italy*

⁴*Laboratory for Pohang Emergent Materials and Max Plank POSTECH Center for Complex Phase Materials, Pohang University of Science and Technology, Pohang 790-784, Korea*

⁵*Rutgers Center for Emergent Materials, Rutgers University, Piscataway, New Jersey 08854, USA*

⁶*National High Magnetic Field Laboratory, Florida State University, Tallahassee, Florida 32310, USA*

⁷*Department of Physics and Astronomy, University of Tennessee, Knoxville, Tennessee 37996 USA*

(Dated: November 24, 2015)

We combined high field optical spectroscopy and first principles calculations to analyze the electronic structure of Ni_3TeO_6 across the 53 K and 9 T magnetic transitions, both of which are accompanied by large changes in electric polarization. The color properties are sensitive to magnetic order due to field-induced changes in the crystal field environment, with those around Ni1 and Ni2 most affected. These findings advance the understanding of magnetoelectric coupling in materials in which magnetic 3d centers coexist with non-magnetic heavy-chalcogenide cations.

PACS numbers: 78.20.Ls, 75.85.+t, 78.40.Ha, 71.20.Ps, 71.70.Ej

Spin and polarization flop transitions are fascinating, especially when controlled by external stimuli like magnetic and electric fields and accompanied by large material responses involving multiple degrees of freedom [1–7]. Multiferroics like MnWO_4 and TbMnO_3 are flagship examples and owe their remarkable properties, including field control of polarization and polarization reversal accompanied by spin-helix reorientation, to the heavy ions that bring strong spin-orbit coupling and magnetic anisotropy [8–11]. Ni_3TeO_6 drew our attention due to the presence of both 3d and 5p cations and an unusual spin-flop transition [12–14]. This system displays a complex magnetic phase diagram in magnetic field and temperature (Fig. 1). A magnetically induced electric polarization ($P = 3,280 \mu\text{C}/\text{m}^2$) arises in the antiferromagnetic I (AFM I) phase below $T_N = 53 \text{ K}$ due to Heisenberg exchange striction in the polar structure, and a peculiar continuous spin-flop transition occurs at 9 T into the AFM II phase, altering the polarization ($\Delta P = 290 \mu\text{C}/\text{m}^2$ at 2 K) [13]. Moreover, Ni_3TeO_6 sports the largest linear magnetoelectric coupling constant in a single-phase material known to date ($\alpha = 1,300 \text{ ps}/\text{m}$) [13]. Metamagnetic transitions accompanied by extraordinarily large polarization changes have been discovered at 52 and 70 T [15], and the indications of a yet unknown magnetic transition between 30 and 35 T were observed [16]. The colossal polarization, rich magnetic phase diagram and large spin-orbit coupling due to incorporation of the heavy Te centers raise the possibility of large dynamic magnetoelectric coupling in this system.

In this Letter, we reach beyond static probes of magnetoelectric coupling in Ni_3TeO_6 to reveal the dynamic interactions between spin and charge sectors. Specifi-

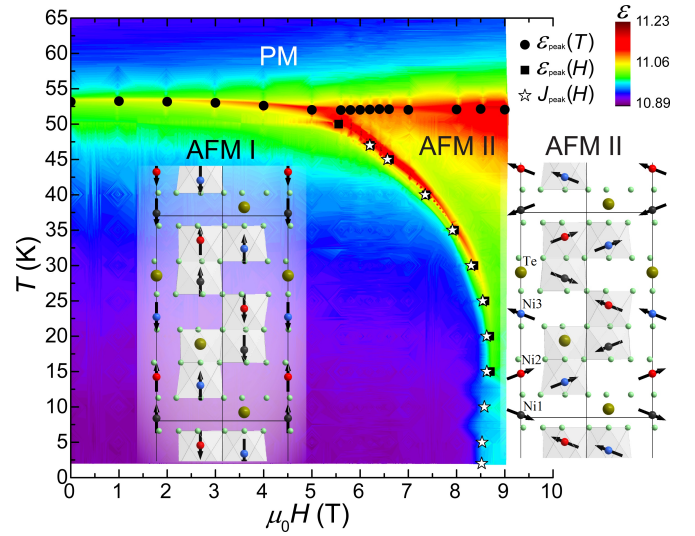


FIG. 1. (Color online) Phase diagram of Ni_3TeO_6 (temperature T vs. magnetic field H) determined by variations in the experimental dielectric constant ϵ (color scale at upper right) and magnetoelectric current. Closed circles, closed squares, and open asterisks indicate peak-center positions for $\epsilon(T)$, $\epsilon(H)$, and magnetoelectric current $J(H)$, respectively [13]. These peaks map the boundaries between the paramagnetic (PM) phase and antiferromagnetic phases (AFM I, AFM II). The structure of Ni_3TeO_6 is of the corundum type with a polar $R3$ space group, three inequivalent $S=1$ Ni sites along c , and significant distortions of oxygen octahedra surrounding Ni ions [12]. The spin configurations in the AFM I and AFM II phases are shown schematically in the insets.

cally, we combined optical property measurements and first principles calculations to uncover interband transitions above 2 eV and a series of Ni d -to- d excitations below 3 eV that are sensitive to magnetic order, evi-

dence that spin-charge coupling persists to much higher energies than previously supposed. Moreover, by analyzing how the color band excitations change with magnetic field, we reveal how and why the crystal field environments – particularly around the Ni1 and Ni2 centers – respond to different microscopic spin arrangements and that polarization and dielectric constant changes across the 9 T transition (Fig. 1) have counterparts at higher energies [16]. Materials that possess large generalized susceptibilities (i.e. strong responses to small stimulus) are promising candidates for spintronic devices [17].

High quality single crystals were grown as described previously [13] and polished to thicknesses of $\approx 28 \mu\text{m}$. Optical transmittance was measured as a function of temperature in the *ab*-plane and along the *c*-direction using a series of spectrometers (0.4-3.0 eV; 4.2-300 K). Absorption was calculated as $\alpha(E) = -(1/d)\ln T(E)$, where $T(E)$ is the transmittance and d is the sample thickness. Magneto-optical measurements were carried out at the National High Magnetic Field Laboratory in Tallahassee, Florida (4.2 K, 0 - 35 T). The first-principles calculations were performed using the Elk full-potential code using linearized augmented plane-wave basis [18], LDA+U in the fully localized limit [19] with Slater parameters $F^{(0)} = 8.0 \text{ eV}$, $F^{(2)} = 8.18 \text{ eV}$, $F^{(4)} = 5.11 \text{ eV}$ [20], and the Perdew-Wang/Ceperley-Alder exchange-correlation functional [21]. The 20-atom rhombohedral magnetic unit cell with the $\uparrow\uparrow\downarrow\downarrow\uparrow$ magnetic ordering was used in the calculations, and a $4 \times 4 \times 4$ k-point grid was employed for reciprocal-space sampling.

Figure 2 displays the absorption of Ni_3TeO_6 in the *ab*-plane and *c*-direction at 300 and 4.2 K. We clearly observe two broad bands below 2 eV. Focusing first on the *ab*-plane data in Fig. 2(a), we find color band excitations near 1.0, 1.55, and 1.72 eV. Each appears with significant oscillator strength due to non-centrosymmetric local environments around each of the Ni sites. Combined with the absorption minimum near 2.25 eV and small shoulder at 2.5 eV, these features are responsible for the striking green color of the crystal. The absorption rises sharply above 2.6 eV, suggesting the start of strong interband transitions.

To test whether the lower-energy peaks might arise from interband transitions, we calculated the Kohn-Sham band structure at the LDA+U level for Ni_3TeO_6 in the zero-temperature antiferromagnetic configuration. The results are shown in Fig. 3, and where comparable, they are in excellent agreement with Ref. 14. The gap, clearly visible in the density of states plot in Fig. 3(a), is determined to be 2.2 eV, which rules out any interband transitions below 2 eV. To drive this point home, the components of LDA+U optical dielectric response tensor calculated within the random phase approximation in the $q \rightarrow 0$ limit are plotted in Fig. 3(c). The interband transitions naturally account for the sharply rising absorption near 2.6 eV (Fig. 2(a)). They are dominated

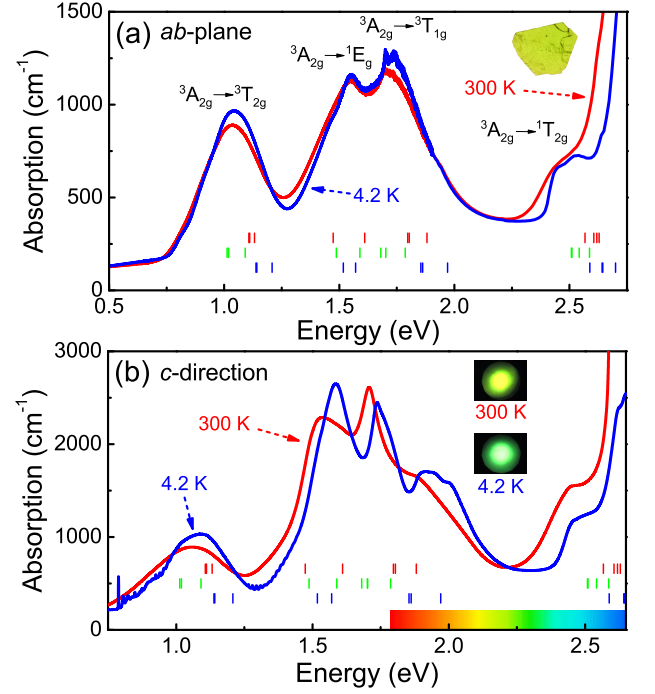


FIG. 2. (Color online) (a) Absorption coefficient of Ni_3TeO_6 , $\alpha(E)$, in the *ab*-plane at 300 and 4.2 K. The inset shows a photograph of the *ab*-plane crystal polished to $28 \mu\text{m}$. Vertical lines near the bottom mark the computed *d*-to-*d* excitations for the d^8 Ni ions, with red, green, and blue indicating excitations on Ni1, Ni2, and Ni3 sites, respectively. (b) Absorption coefficient of Ni_3TeO_6 in the *c* direction at 300 and 4.2 K. The insets show photographs of the crystal at these temperatures.

by excitations from hybridized O *p* and majority Ni e_g states at the top of the valence band to Te *s* and minority Ni e_g conduction bands. We therefore assign the features below 2 eV to on-site Ni *d*-to-*d* excitations, an assignment that is strengthened by the resemblance to $\text{Ni}_3\text{V}_2\text{O}_8$ [5], where similar *d*-to-*d* transitions occur and where the charge-transfer gap of 2.4 eV is only slightly smaller than ours. We shall give further theoretical support for this assignment shortly.

Returning to the experimental data and focusing now on comparing the *c*-axis response of Ni_3TeO_6 shown in Fig. 2(b) with the in-plane data of Fig. 2(a), we immediately notice that while the intensities of the 1.2 eV peaks are similar, there is a large anisotropy of the response between 1.5 and 2.2 eV, with the absorption being much stronger along *c* ($\approx 2500 \text{ cm}^{-1}$) than in the *ab* plane ($\approx 1300 \text{ cm}^{-1}$). The temperature effects are also more interesting in this direction, with the 4.2 K data showing (i) an overall hardening of the excitations, (ii) an intensity increase near 1.9 eV, and (iii) fine structure on the leading edge of the 1.1 eV band that may correspond to a series of phonon side bands [16]. Examination of the 1.9 eV excitation reveals that the peak shape is a strong function of temperature. In fact, the additional

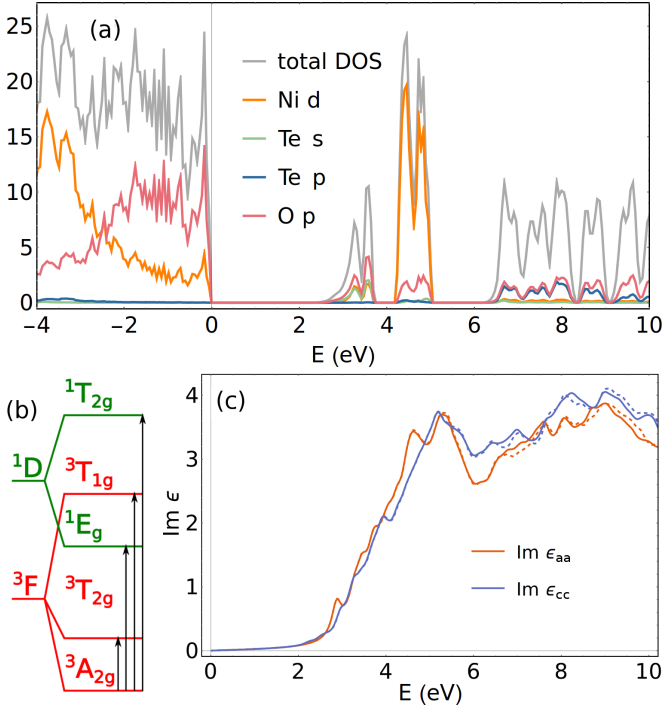


FIG. 3. (Color online) Results of DFT calculations on Ni_3TeO_6 : (a) ion-projected density of states per magnetic unit cell, (b) splitting of free Ni ion d^8 multiplets in the presence of an octahedral crystal field and the crystal field excitations between these levels, and (c) components of linear optical dielectric response tensor calculated within the random phase approximation in the $q \rightarrow 0$ limit with no microscopic contributions (solid lines: with spin-orbit coupling included; dashed: without).

absorption of orange light at 4.2 K might be expected to cause Ni_3TeO_6 appear more green to the naked eye. Direct photographic images (inset, Fig. 2(b)) verify this supposition.

As noted above, we have assigned the color-band excitations below 2.5 eV to on-site d -to- d transitions, which are not expected to appear in a single-particle framework such as DFT+U. To confirm this assignment, we turn to a crystal field model. The Coulomb interactions for a spherically symmetric d^8 ion give rise to the ground state 3F . These are correlated states that generally cannot be represented as a single Slater determinant. In particular, the state with the largest orbital moment, 2^+2^- , where both holes in the d shell have $m_l = 2$ and opposite spins (indicated by superscripts “+” and “-”), is a single Slater determinant. Instead, the state obtained by applying the angular momentum lowering operator L^- , and thus belonging to the same multiplet, is made up of the microstates 2^+1^- and 2^-1^+ , and so is not a single-determinant state [22, 23]. The next multiplet is 1D , followed by 3P , 1G , and 1S states. In the (approximately) octahedral crystal field of the oxygen cage surrounding the Ni ions, the lowest multiplet splits as $^3F \rightarrow$

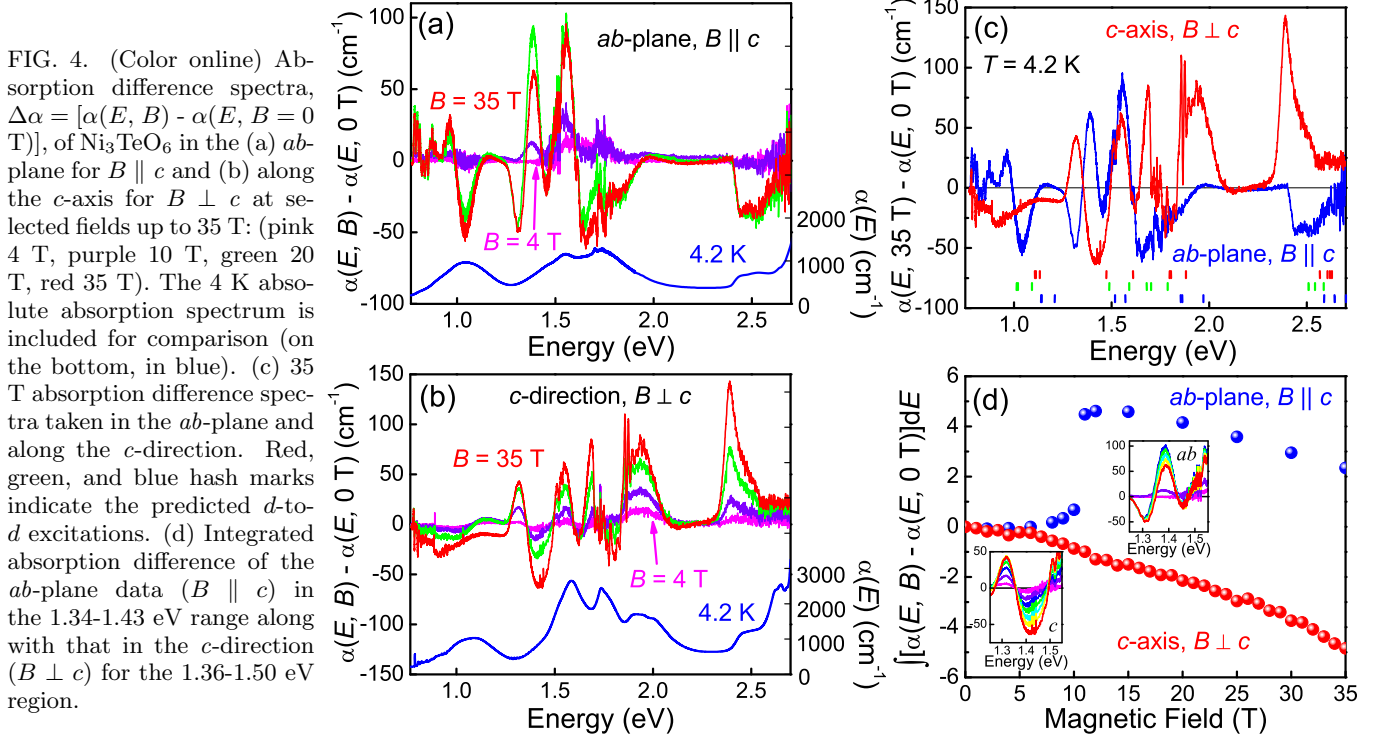
$\Gamma_2 = ^3A_{2g}$ ($E = -12Dq$), $\Gamma_5 = ^3T_{2g}$ ($E = -2Dq$), and $\Gamma_4 = ^3T_{1g}$ ($E = 6Dq$), where $10Dq$ corresponds to the splitting of a single d -level that would be produced by the same octahedral crystal field. The next lowest multiplet splits as $^1D \rightarrow \Gamma_3 = ^1E_g$ ($E = 5F_2 + 45F_4 - \frac{24}{7}Dq$) and $^1T_{2g}$ ($E = 5F_2 + 45F_4 + \frac{16}{7}Dq$). These splittings are shown schematically in Fig. 3(b), where the vertical black arrows indicate the optical excitations of interest.

In order to estimate the d -to- d transition energies for Ni_3TeO_6 , we performed exact diagonalization of an atomic Hamiltonian in the d^8 sector for each of the three inequivalent Ni sites. The Hamiltonian included the Hund’s exchange energy, $J_H = 0.9$ eV, and the orbital energies in the crystal field, approximated by the energies of Wannier functions obtained from the DFT calculations for each of the three Ni ions. The vertical marks in Fig. 2 show that these predicted excitation energies coincide well with the peaks observed in our experiment. The excitations near 1.0, 1.55, 1.72, and above 2.5 eV are therefore associated with transitions to the Γ_5 , Γ_3 , Γ_4 , and Γ_5 multiplets, respectively. This confirms the interpretation of the absorption bands below 2 eV as resulting from d -to- d transitions. The assignment also clarifies that the shoulder near 2.5 eV is related to on-site excitations and not yet the beginning of the interband transitions. This framework and the position of the spectral peaks allow us to estimate that Dq and the Racah parameter B are both (coincidentally) equal to 0.11 eV, consistent with expectations for a Ni^{2+} complex [24].

We now turn to the optical response in applied field. Figures 4(a) and (b) summarize the magneto-optical properties of Ni_3TeO_6 in the ab -plane ($B \parallel c$) and in the c -direction ($B \perp c$) at 4.2 K. The data are displayed as a set of absorption difference spectra, $\Delta\alpha(E, B) = \alpha(E, B) - \alpha(E, B = 0)$, for selected fields ranging from 4 to 35 T. The zero-field linear absorption $\alpha(E)$ is also shown at the bottom of each panel for reference. In general, the size of $\Delta\alpha$ increases with field, although the peak near 1.4 eV (related to changes in $^3A_{2g} \rightarrow ^1E_g$ excitations) is an exception.

Figure 4(c) brings together the full field absorption difference spectra, $\Delta\alpha(E, B) = \alpha(E, B = 35 \text{ T}) - \alpha(E, B = 0 \text{ T})$, with the theoretical locations of the three different sets of d -to- d transitions indicated at the bottom as in Fig. 2. Comparison of these spectra with the predicted crystal-field excitations verifies that the observed features are due to field-induced changes in the Ni d -to- d excitations.

Inspection of Fig. 4(a) reveals that the ab -plane absorption difference spectra ($B \parallel c$) display a sharp discontinuity across the 9 T spin flop transition. This discontinuity is not seen in the c -axis data of Fig. 4(b), which is not surprising since these were taken with $B \perp c$ where the spin-flop transition does not occur. Figure 4(d) quantifies these trends by plotting the absorption difference, integrated over an energy window near 1.4 eV, as a func-



tion of magnetic field. The *ab*-plane response to the magnetic field ($B \parallel c$) displays a sharp jump across the 9 T transition, along with some precursor effects (both below and above the spin-flop transition) and no hysteresis (not shown). This indicates that the electronic properties are sensitive to changes in the microscopic spin pattern - a direct consequence of spin-charge coupling and analogous to the dielectric response in Fig. 1. By contrast, in the absence of a spin-flop transition, the *c*-axis response ($B \perp c$) shows only a gradual decrease in the integrated $\Delta\alpha$ with no distinguishing characteristics.

Another interesting aspect of the magneto-optical response is that $\Delta\alpha$ has not saturated by 35 T, suggesting that higher fields are likely to uncover new magnetic phases. Recent magnetization and magneto-infrared experiments do in fact reveal the possibility of an unexplored transition between 30 and 35 T as well as metamagnetic transitions at 52 and 70 T for $B \parallel c$ [15, 16].

A closer examination of the data in Fig. 4 (Supplemental Information) along with an analysis of the local structure [12, 25] unveils the role of each of the three distinct Ni ions. The Ni3 centers, for instance, have a relatively irregular environment and strong crystal field associated with their face-shared proximity to the unusual Te^{6+} cations (structural inset of Fig. 1). We note that this environment correlates with the appearance of *d-to-d* transitions (blue hashes) on the high-energy side of each cluster of predicted excitations, which is precisely the range with little or no magneto-optical response. By contrast, the Ni2 ions have the least distorted environ-

ment and weakest crystal field, and their predicted on-site excitations (green hashes) are at lower energies compared to those of the other two Ni centers. Since absorption difference structures always appear on the leading edge of each band - both in the *ab*-plane and along *c* - we can conclude that Ni2 ions are involved. The same is true for the Ni1-related features, which are in the middle. We therefore surmise that electronic structure changes through the spin flop transition derive from field-induced modifications to the crystal field of Ni1 and Ni2 (and associated changes in hybridization). The 310 cm^{-1} phonon involving Ni1 and Te displacement in the *ab*-plane is sensitive to the 9 T critical field [16] and may help drive these distortions. Recent calculations support the dominant contribution of Ni1...Ni2 interactions to the magnetic properties [14] as well as magnetically induced electric polarization [15].

In summary, we bring together optical spectroscopy and first principles calculations to reveal how and why the electronic properties of Ni_3TeO_6 can be controlled by magnetic field, and we trace the color property tunability to magnetic field-induced changes in specific crystal field environments and their associated Ni *d-to-d* excitations. In addition to providing a superb platform for the exploration of coupled charge and spin degrees of freedom, these findings reveal that the remarkable polarization properties and magnetoelectric coupling in Ni_3TeO_6 extend to much higher energies than previously supposed [13]. We anticipate that this system will become an important prototype in the understanding of

an unusual class of oxides in which transition-metal and heavy-chalcogenide cations coexist, leading to generalized susceptibilities that are controllable with external stimuli.

Research at the University of Tennessee and Rutgers University is supported by the NSF-DMREF program (DMR-1233118 and DMR-1233349). Work at Postech is funded by the Max Planck POSTECH/KOREA Research Initiative Program 2011-0031558 through NRF of Korea funded by MEST. A portion of this research was performed at the National High Magnetic Field Laboratory which is supported by the National Science Foundation Cooperative Agreement DMR-1157490, the State of Florida, and the U.S. Department of Energy.

-
- [1] D. I. Khomskii, *Physics* **2**, 20 (2009).
 - [2] F. Matsukura, Y. Tokura, and H. Ohno, *Nat. Nanotech.* **10**, 209 (2015).
 - [3] W. Eerenstein, N. D. Mathur, and J. F. Scott, *Nature* **442**, 759 (2006).
 - [4] S.-W. Cheong and M. Mostovoy, *Nat. Mater.* **6**, 13 (2007).
 - [5] P. Chen, B. S. Holinsworth, K. R. O’Neal, T. V. Brinzari, D. Mazumdar, Y. Q. Wang, S. McGill, R. J. Cava, B. Lorenz, and J. L. Musfeldt, *Phys. Rev. B* **89**, 165120 (2014).
 - [6] H. Matsuzaki, H. Nishioka, H. Uemura, A. Sawa, S. Sota, T. Tohyama, and H. Okamoto, *Phys. Rev. B* **91**, 081114(R) (2015).
 - [7] N. Poudel, K.-C. Liang, Y.-Q. Wang, Y. Y. Sun, B. Lorenz, F. Ye, J. A. Fernandez-Baca, and C. W. Chu, *Phys. Rev. B* **89**, 054414 (2014).
 - [8] K. Taniguchi, N. Abe, T. Takenobu, Y. Iwasa, and T. Arima, *Phys. Rev. Lett.* **97**, 097203 (2006).
 - [9] O. Heyer, N. Hollmann, I. Klassen, S. Jodlauk, L. Bohaty, P. Becker, J. A. Mydosh, T. Lorenz, and D. Khomskii, *J. Phys. Condens. Matter* **18**, L471 (2006).
 - [10] F. Ye, R. S. Fishman, J. A. Fernandez-Baca, A. A. Podlesnyak, G. Ehlers, H. A. Mook, Y. Wang, B. Lorenz, and C. W. Chu, *Phys. Rev. B* **83**, 140401(R) (2011).
 - [11] T. Aoyama, K. Yamauchi, A. Iyama, S. Picozzi, K. Shimizu, and T. Kimura, *Nat. Commun.* **5**, 4927 (2014).
 - [12] I. Živković, K. Prša, O. Zaharko, and H. Berger, *J. Phys.: Condens. Matter* **22**, 056002 (2010).
 - [13] Y. S. Oh, S. Artyukhin, J. J. Yang, V. Zapf, J. W. Kim, D. Vanderbilt, and S.-W. Cheong, *Nat. Commun.* **5**, 3201 (2014).
 - [14] F. Wu, E. Kan, C. Tian, and M. -H. Whangbo, *Inorg. Chem.* **49**, 7545 (2010).
 - [15] J. W. Kim, S. Artyukhin, E. D. Mun, M. Jaime, N. Harrison, A. Hansen, J. J. Yang, Y. S. Oh, D. Vanderbilt, V. S. Zapf, and S.-W. Cheong, *Phys. Rev. Lett.* **115**, 137201 (2015).
 - [16] M. O. Yokosuk, S. Artyukhin, A. al-Wahish, X. Wang, J. Wang, Z. Li, S.-W. Cheong, D. Vanderbilt, J. L. Musfeldt, *Phys. Rev. B* **92**, 144305 (2015).
 - [17] S. A. Wolf, D. D. Awschalom, R. A. Buhrman, J. M. Daughton, S. von Molnár, M. L. Roukes, A. Y. Chtchelkanova, and D. M. Treger, *Science* **294**, 1488 (2001).
 - [18] K. Dewhurst, S. Sharma, L. Nordström, F. Cricchio, F. Bultmark, O. Grånäs, H. Gross, C. Ambrosch-Draxl, C. Persson, C. Brouder, *et al.* The Elk FP-LAPW Code [Online]. 2015. <http://elk.sourceforge.net> [July 2015].
 - [19] F. Bultmark, F. Cricchio, O. Grånäs, and L. Nordström, *Phys. Rev. B* **80**, 035121 (2009).
 - [20] V. I. Anisimov, I. V. Solovyev, M. A. Korotin, M. T. Czyżyk, and G. A. Sawatzky, *Phys. Rev. B* **48**, 16929 (1993).
 - [21] J. P. Perdew and Y. Wang, *Phys. Rev. B* **45**, 13244 (1992).
 - [22] C. J. Ballhausen, *Introduction to Ligand Field Theory*, McGraw-Hill Book Co., Inc. 1962
 - [23] R. Eder, Multiplets in transition metal ions, in E. Pavarini, E. Koch, F. Anders, and M. Jarrell (eds.) *Correlated Electrons: From Models to Materials Modeling and Simulation*, Vol. 2 Verlag des Forschungszentrum Jülich, 2012.
 - [24] S. L. Reddy, T. Endo, and G. S. Reddy, *Electronic (Absorption) Spectra of 3d Transition Metal Complexes*, in M. A. Farrukh (ed.) *Advanced Aspects of Spectroscopy*, InTech, 2012.
 - [25] Ni1 is strongly distorted, Ni2 is the most symmetric C₃ site, and Ni3 is the most distorted of all [12].

Supplementary information for “Magnetoelectric coupling through the spin flop transition in Ni_3TeO_6 ”

M. O. Yokosuk,¹ Amal al-Wahish,¹ Sergey Artyukhin,² K. R. O’Neal,¹ D. Mazumdar,¹ P. Chen,¹ Junjie Yang,³ Yoon Seok Oh,^{2,4} Stephen A. McGill,⁵ K. Haule,² Sang-Wook Cheong,^{2,3,4} David Vanderbilt,² and J. L. Musfeldt^{1,6}

¹*Department of Chemistry, University of Tennessee, Knoxville, Tennessee 37996 USA*

²*Department of Physics and Astronomy,*

Rutgers University, Piscataway, New Jersey 08854, USA

³*Laboratory for Pohang Emergent Materials and Max*

Plank POSTECH Center for Complex Phase Materials,

Pohang University of Science and Technology, Pohang 790-784, Korea

⁴*Rutgers Center for Emergent Materials,*

Rutgers University, Piscataway, New Jersey 08854, USA

⁵*National High Magnetic Field Laboratory,*

Florida State University, Tallahassee, Florida 32310, USA

⁶*Department of Physics and Astronomy,*

University of Tennessee, Knoxville, Tennessee 37996 USA

Figure S1 shows the absorption spectra of Ni_3TeO_6 in the ab -plane and along c at 0 and 35 T. The full field data was back-calculated by adding the absorption difference curve at 35 T (calculated as $\Delta\alpha = \alpha(E, B = 35 \text{ T}) - \alpha(E, B = 0 \text{ T})$) to the spectrum taken at 0 T. As in the main text, the absorption difference spectrum is plotted for comparison. Because the three Ni ions have different local environments (and therefore different crystal field splittings), each set of Ni d -to- d excitation energies is distinct. Since the Ni3 environment is most distorted from a perfect octahedral environment, it has the largest crystal field splitting, and the predicted excitations emanating from these sites have the overall highest energies. By contrast, the Ni2 centers have the least distortion, the smallest crystal field splitting, and the overall lowest energies within each cluster of excitations.

It’s easy to see from Fig. S1 that the optical properties of Ni_3TeO_6 change with applied

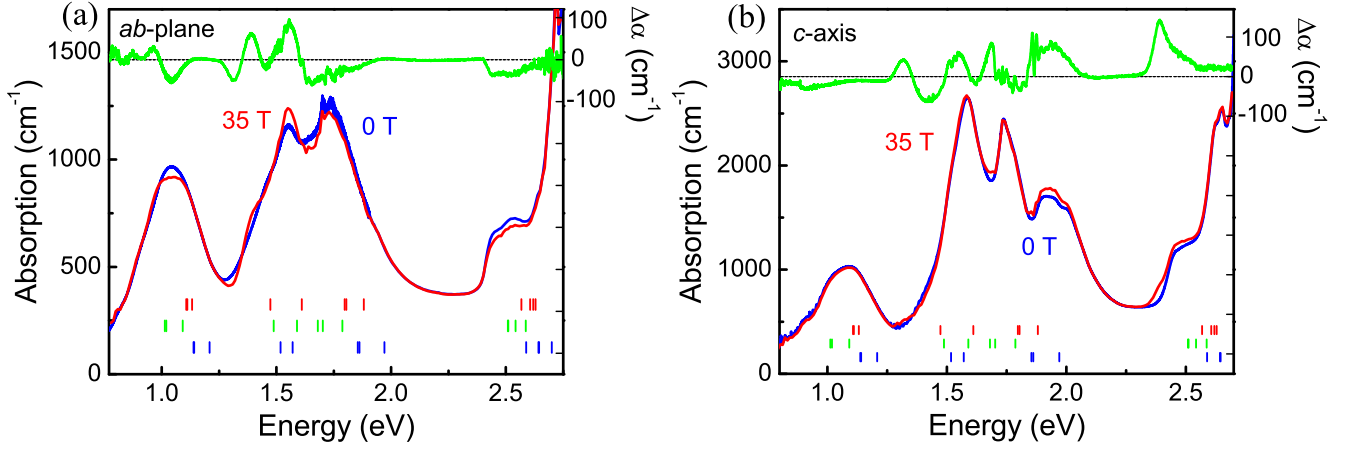


FIG. S1: (a) Absolute absorption spectrum of Ni₃TeO₆ at 0 and 35 T in the *ab*-plane along with the full field absorption difference at 4.2 K. (b) Absorption spectrum at 0 and 35 T in the *c*-direction along with the absorption difference given by $\Delta\alpha = \alpha(E, B = 35 \text{ T}) - \alpha(E, B = 0 \text{ T})$, at 4.2 K. The vertical tick marks at the bottom of each graph indicate the predicted *d*-to-*d* excitation energies of each of the Ni centers (Ni1 in red, Ni2 in green, Ni3 in blue).

field. A closer view is, however, required to link these modifications with distortions and the associated crystal field splittings around each of the Ni centers. For comparison, each cluster of excitations (both predicted and measured) is shown separately in Figs. S2 and S3. While some energy windows are more revealing than others, several general trends emerge. For instance, in the majority of cases, the leading edge of the band (and sometimes other energy windows near the center) are affected by magnetic field. This suggests that the local environment around Ni2 (and probably Ni1 as well) is changing. By contrast, the trailing edge of each of the bands has very limited or no field dependence. Since we know (based upon the predicted sequence of excitations) that the *d*-to-*d* excitations emanating from the Ni3 centers always govern the shape of the band tail, we surmise that the local structure around the Ni3 centers is not very sensitive to magnetic field. This is probably because the Ni3 site is already strongly distorted. These findings are in excellent agreement with the predictions of Wu *et al.* on the importance of superexchange within the Ni1⋯Ni2 pair to the magnetic properties [S1].

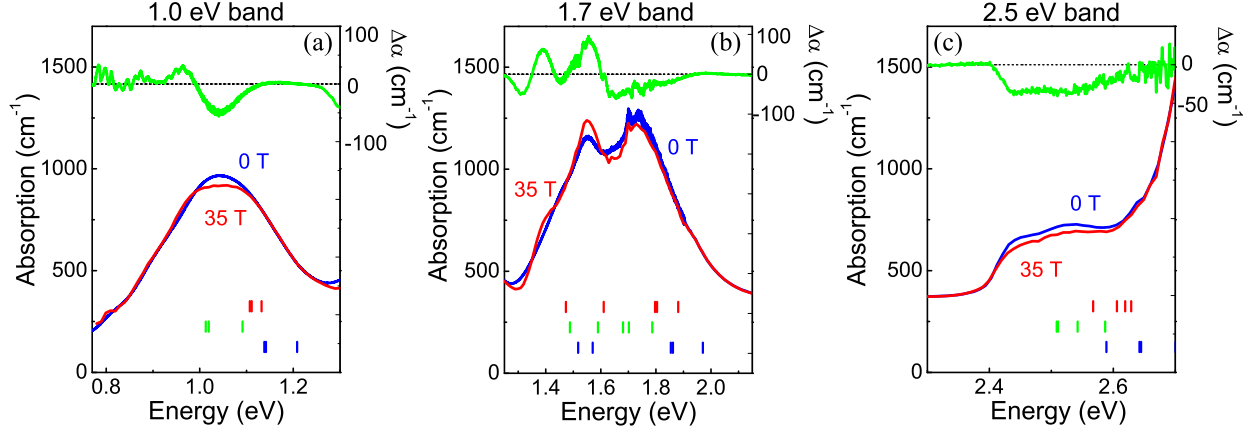


FIG. S2: Close-up views of the Ni *d*-to-*d* excitations in the vicinity of the (a) 1.0, (b) 1.7, and (c) 2.5 eV bands in the *ab*-plane. The set of vertical tick marks show the calculated excitations for each type of Ni center (Ni1 in red, Ni2 in green, Ni3 in blue). As discussed here and in the main text, the relative position of these excitations reveals the relative size of the crystal field splitting.

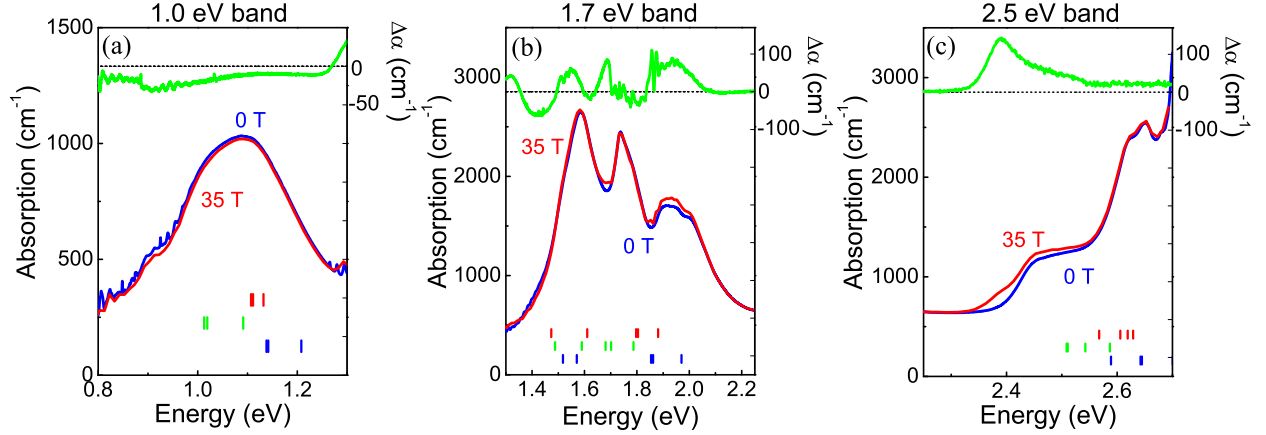


FIG. S3: Close-up views of the Ni *d*-to-*d* excitations in the vicinity of the (a) 1.0, (b) 1.7, and (c) 2.5 eV bands in the *c*-direction. The set of vertical tick marks at the bottom of each panel indicate the calculated excitations for each type of Ni center (Ni1 in red, Ni2 in green, Ni3 in blue) [S2].

[S1] F. Wu, E. Kan, C. Tian, and M. -H. Whangbo, *Inorg. Chem.* **49**, 7545 (2010).

[S2] Additional resolution is required to track changes in the exciton and phonon sidebands in applied field.